REPORT DOCUMENTATION PAGE

AFRL-SR-BL-TR-01-

0281

1. REPORT DATE (DD-MM-YYYY)	2. REPORT TYPE	3. DATES COVERED (From - To)
22/02/2001	Final technical report	6/1/97-5/31/00

4. TITLE AND SUBTITLE
AASERT - Fabrication and Characterization of Photoconductive AlGaN Detectors / Structural Characterization of SiC WAfers

5a. CONTRACT NUMBER
F49620-97-1-0452

5b. GRANT NUMBER

5c. PROGRAM ELEMENT NUMBER

6. AUTHOR(S)
Marek Skowronski

5d. PROJECT NUMBER

5e. TASK NUMBER

5f. WORK UNIT NUMBER

7. PERFORMING ORGANIZATION NAME(S) AND ADDRESS(ES)

Carnegie Mellon University
Schenley Park
Pittsburgh, PA 15213

8. PERFORMING ORGANIZATION REPORT NUMBER

9. SPONSORING / MONITORING AGENCY NAME(S) AND ADDRESS(ES)
AFOSR/NE, 801 North Randolph Street, Arlington VA 22203
Contract monitor:
Maj. D. K. Johnstone

10. SPONSOR/MONITOR'S ACRONYM(S)
AFOSR

11. SPONSOR/MONITOR'S REPORT NUMBER(S)

12. DISTRIBUTION / AVAILABILITY STATEMENT

APPROVED FOR PUBLIC RELEASE,
DISTRIBUTION UNLIMITED

AIR FORCE OFFICE OF SCIENTIFIC RESEARCH (AFOSR)
NOTICE OF TRANSMITTAL DTIC. THIS TECHNICAL REPORT
HAS BEEN REVIEWED AND IS APPROVED FOR PUBLIC RELEASE
LAW AFR 190-12. DISTRIBUTION IS UNLIMITED.

13. SUPPLEMENTARY NOTES

14. ABSTRACT

Structure of silicon carbide wafers have been evaluated by x-ray topography, high resolution x-ray diffraction, etching, Atomic Force Microscopy, and related techniques. The low angle grain boundaries were imaged by White Beam Synchrotron X-Ray Topography and mis-orientations quantitatively mapped out by x-ray diffraction. The dominant component of mis-orientation was basal plane tilt. The formation mechanism is most likely due to buckling of the rigidly mounted SiC seed during initial stages of growth. The morphology of hexagonal voids was studied by optical microscopy and AFM. Voids originate at the seed crystal / crucible lid interface and move through the boule during growth. Interaction of void and grown in dislocations leads to formation of dislocation arrays and open core screw dislocations underneath the void. It appears to be the dominant formation mechanism of micropipes.

15. SUBJECT TERMS
silicon carbide, structure, dislocation

16. SECURITY CLASSIFICATION OF:			17. LIMITATION OF ABSTRACT	18. NUMBER OF PAGES	19a. NAME OF RESPONSIBLE PERSON
a. REPORT	b. ABSTRACT	c. THIS PAGE			19b. TELEPHONE NUMBER (include area code)
unclassified	unclassified	unclassified		22	

Final Technical Report

AFOSR Grant F49620-97-1-0452

June 1, 1997 –May 1, 2000

Marek Skowronski

Department of Materials Science and Engineering

Carnegie Mellon University

Pittsburgh, PA 15213

Research objectives

The initial objectives of this project were centered on "Fabrication and Characterization of Photoconductive and pn Junction-Based AlGaN Detectors" and were aligned with the objective of the "parent" grant entitled "Growth of Lattice Matched Nitride Alloys and Structures" (Grant # F49629-95-1-0087). However, since the parent grant was terminated due to budget cuts at Air Force Office of Scientific Research these objectives have been changed. The new research goals are aligned with goals of several projects funded by Air Force Research Laboratory at Carnegie Mellon University including "Growth of semi-insulating 4H-SiC crystals for GaN-based microwave device substrates" POC: L. S. Rea phone: (937) 255-4474 ext. 3213; "High Volume, High Quality Silicon Carbide Substrate Merchant Manufacturing" subcontract to Sterling Semiconductor, Inc., and "Three Inch SiC substrate manufacturing", subcontract to Airtron Litton Corporation, Air Force Title III program, POC: J. Blevins, Air Force Research Laboratory, (937) 255-3701 ext. 226.

The major goal of the project is structural characterization of SiC (SiC) wafers provided by Air Force Research Laboratories (deliverables for DARPA programs). The structural quality of silicon carbide wafers is poorly characterized and even less understood. It is known, however, that the boules contain following defects:

(i) micropipes - open core screw dislocations propagating along the c-axis of hexagonal polytypes of SiC. The typical density of this defect is between 10-1000 cm^{-2} in commercially available wafers.

(ii) Elementary screw dislocations with the Burgers vector c[0001] also propagating along the growth axis. Most wafers exhibit screw dislocation densities in 10^3-10^4 cm^{-2} range.

(iii) Threading edge dislocations with Burgers vector a/3<11-20> and dislocation line direction along [0001]. Threading edges are present in densities between 10^4-10^5 cm^{-2}.

(iv) Basal plane dislocations with Burgers vector a/3<11-20>. The preferred dislocation line direction is also within the basal plane and along equivalent direction <11-20>. This makes most of the basal plane dislocations a 60°-type. The density of this defect is not reported but is expected to exceed 10^5 cm^{-2} in axially cut slices (basal plane dislocations do not intersect the wafer surface for on-orientation wafers which makes it difficult to detect them).

(v) Low angle grain boundaries resulting in multiple peaks in the basal plane x-ray diffraction. Typical misorientations are between 10 and 1000 arc seconds.

(vi) Hexagonal platelet-shape voids. The Cree Research specification limits the total area of hexagonal voids in a wafer to below 10%.

(vii) Macro-pores – tubular-shape cavities with diameter of 10-100 μm, frequently the walls of these voids contain un-bonded carbon.

(viii) Inclusions – both types of intrinsic inclusions have been reported (silicon and carbon). In addition, metallic impurities are known to form inclusions as well.

This project focused on three of the above defects, namely: low angle grain boundaries (v), macro-pores (vii), and hexagonal voids (vi). Project has made significant contributions to the understanding of the origin of these defects, proposed specific approaches to their elimination and/or reduction, and in two cases demonstrated a practical and reliable way of defect elimination. As proposed the tools used included high resolution x-ray diffraction mapping, x-ray topography, KOH etching, and Atomic Force Microscopy for defect assessment and identification.

Summary of research performed

Low angle grain boundaries

One of the characteristic features frequently observed in silicon carbide wafers produced by all manufacturers are radial lines visible either in x-ray topography images or in form of etch pit arrays on the silicon faces of KOH-etched wafers. Two examples of such lines observed in 3 inch diameter experimental wafers obtained from Cree Research are shown in Fig. 1. The wafers were cut on axis and double-side polished. Back-reflection topographs were taken at the Stony Brook Synchotron Topography Facility, Beamline X-19C, at the National Synchotron Light Source, at Brookhaven National Laboratory. Prominent features in both images include dark lines (D) having a radial distribution around a more highly contrasted center region, and clusters of white spots that have been previously determined to correspond to micropipes and elementary screw dislocations [1]. In Fig. 1(a), the dark lines extend from the center of the wafer along the $<11\bar{2}0>$ and $<1\bar{1}00>$ crystallographic directions, whereas in Fig. 1(b) the lines have a more even radial distribution and do not necessarily originate at the center of the wafer. In Fig. 1(b) there are also two partial rings (R) that bisect the shorter dark line segments, indicating an additional type of deformation not apparent in Fig. 1(a).

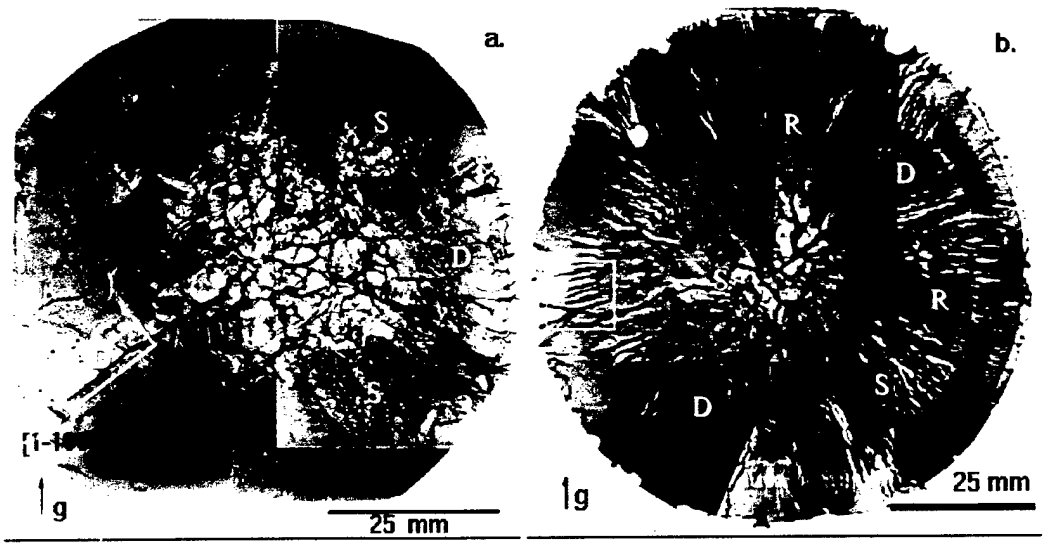

Fig. 1 Back-reflection topographs of experimental 3 inch SiC wafers. (a) 4H(00016), λ=1.26 Å and (b) 6H(00024), λ=1.26 Å.

The ω-2θ scans performed by high resolution x-ray diffraction on either of the two wafers revealed only one well defined position of the [0006] or [0008] reflection with the half width of approximately 20 arc seconds. This result indicates that neither one of the two wafers had any foreign polytype inclusions or strains that would affect the c lattice parameter. The entire contrast in the topographs above must originate in misorientations of the basal plane. More specifically the only two out of three possible misorientations could produce the contrast in topographs: the tilt and rotation around axis contained in the basal plane. These two components will be referred to as tilt and twist, respectively, in the remainder of this report. The third component, namely, rotation around the c-axis should not affect the basal plane reflection.

The magnitude of both components of misorientation was measured by High Resolution X-Ray Diffraction (HRXRD) mapping. The first characteristic feature that was investigated with HRXRD is a long radial dark line visible in Fig. 1a and marked with the letter D. Both the segment of back-reflection topograph and corresponding HRXRD map with the ω rotation axis in the basal plane are shown in Fig. 2.

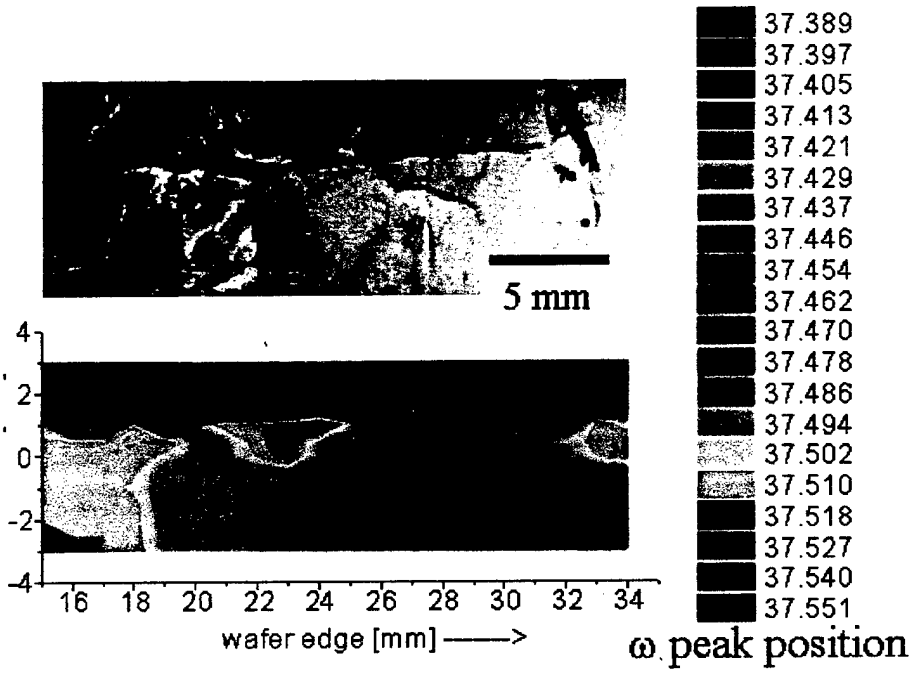

Fig. 2 Enlarged part of the back-reflection topograph shown in Fig. 1(a) (upper part) and corresponding false color map of ω peak positions for (0008) reflection with the rocking axis along the boundary (tilt misorientation component, lower map).

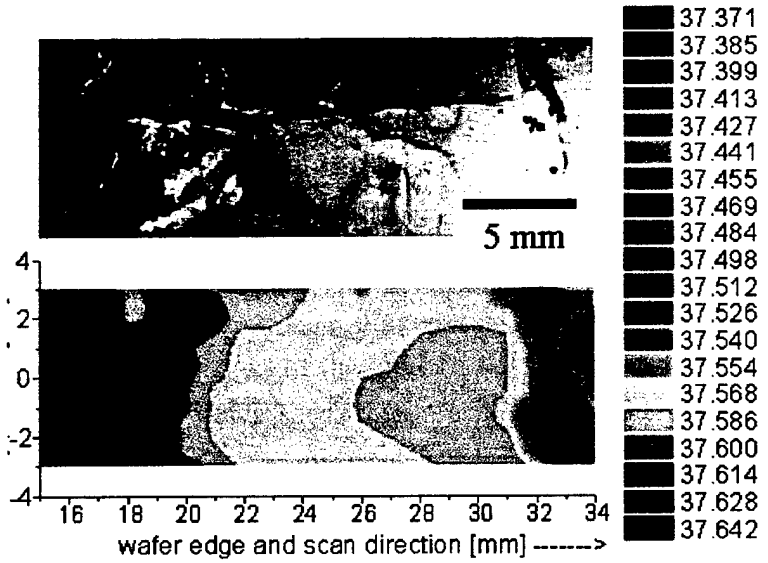

Fig. 3 Enlarged part of the back-reflection topograph shown in Fig. 1 (a) (upper part) and corresponding false color map of ω peak positions for (0008) reflection with the rocking axis perpendicular to the boundary direction (twist misorientation component, lower map).

The HRXRD maps have been generated by plotting the ω peak position of the absolute intensity maximum of an individual rocking curves. The resulting map shows the change in orientation of the basal planes along the directions perpendicular to the rocking axis. In Fig. 2, the rocking axis is parallel to the defect line, thus being sensitive to the tilt component across the boundary. In Fig. 3, the rocking axis is perpendicular to the boundary, thus being sensitive to twist along the boundary. The boundary is clearly visible in Fig. 2 but not in Fig. 3, indicating that the boundary has only a tilt component with rotation axis in the basal plane. Fig. 3 shows a uniform bending of the basal planes toward the outer edge of the wafer that was not associated with this specific defect, but present over much of the wafer. The misorientation across the boundary is greatest near the center of the wafer at a value of 540 arc sec and decreases to near zero at the outer edge of the wafer. A similar defect lying along the $[11\bar{2}0]$ (on the right side of Fig. 1a) was also shown to be a tilt boundary by HRXRD. The wafer was cleaved across the boundary, and the $(1\bar{1}00)$ planes of the wafer cross-section were examined to determine the second component of tilt that might be associated with the boundary, but misorientations associated with other defects close by masked any misorientation that may be associated with the boundary under examination.

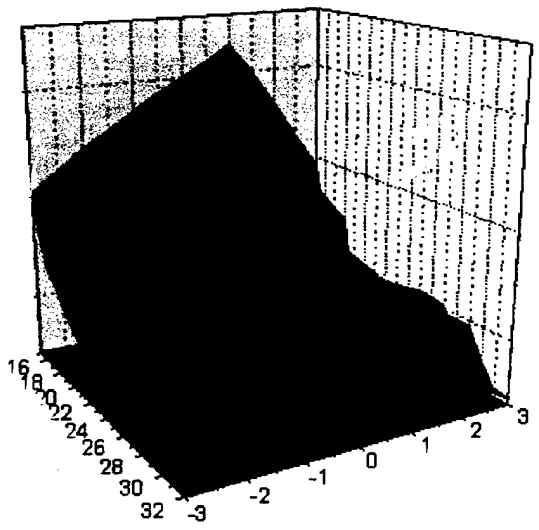

Fig. 4 Real space orientation of basal plane in the 4H-SiC wafer (based on the integrated data in Fig. 2 and 3).

Two common types of dislocation arrays can produce misorientations that affect basal plane reflections; basal plane dislocations stacked above one another, or threading screw dislocations. Only basal plane dislocations can produce the pure tilt boundary shown in Fig. 2. Etching of the Si-face revealed micropipes and threading dislocations in several arrays on various areas of the wafer, but not above the known locations of the grain boundaries, indicating that the boundaries are likely to be composed of basal plane dislocations. We are attempting to do a cross-sectional Transmission Electron Microscopy on such boundaries to obtain direct experimental identification of defects making up the boundary.

Fig. 5 and 6, show the same sequence of images for the second 6H-SiC wafer. As can be seen in Fig. 5, a region not containing the black ring on the left side of Fig. 1(b) was used to simplify the interpretation of the contrast associated with the dark lines. Figs. 5 and 6 show that there is more than one component of misorientation associated with each defect line even without the presence of the dark ring. One reason that the HRXRD maps do not show the same scale of detail as in the topograph could be that the beam footprint is larger than the distance between the boundaries. KOH etching of the second wafer revealed etch pits that closely matched the contrast in the topograph. These etch pits could be associated with threading dislocations adding a twist component to the misorientation. It is important to note that the orientation change across each radial boundary line in a circular trace around the wafer alternates between a positive and negative change in position, giving a zigzag shape to the basal planes in the line of the trace. The range of misorientations in the 6H wafer is approximately 500 arcsec, as shown in Figs. 4 and 5. The third component of misorientation (second tilt) was not measured.

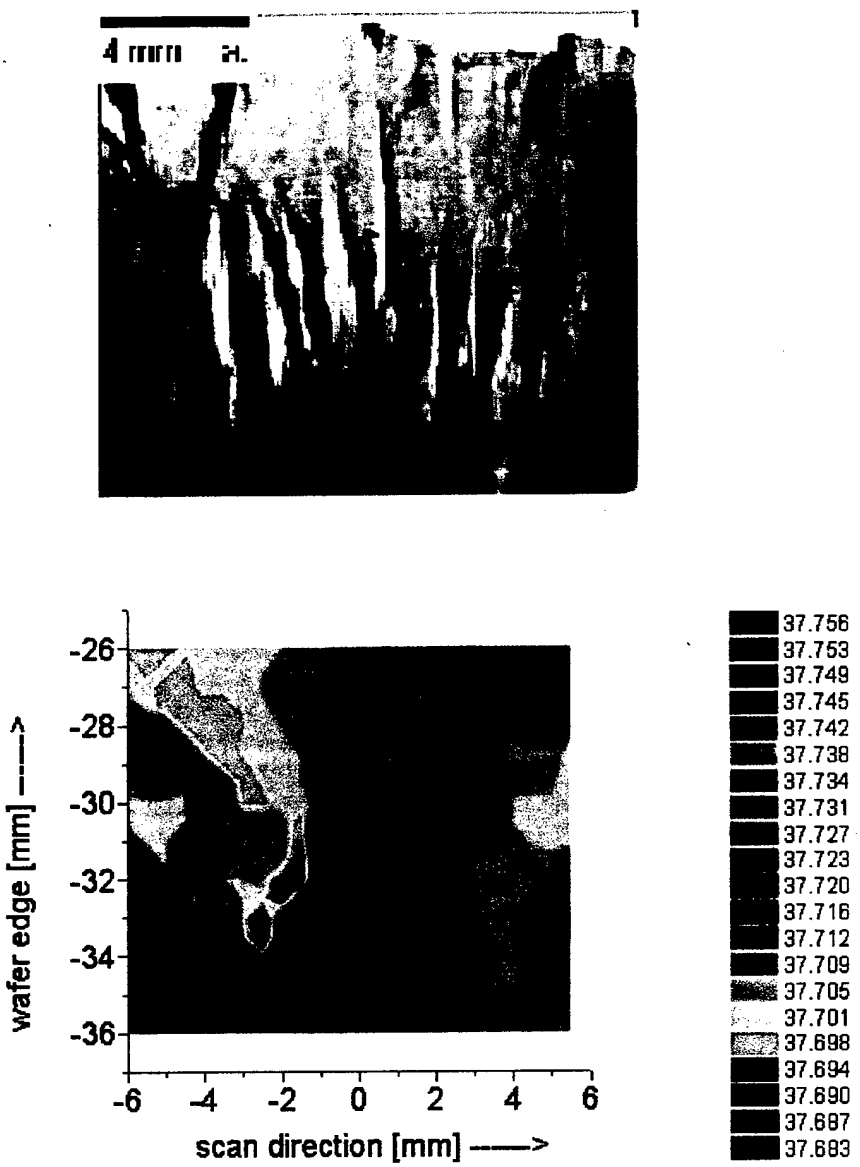

Fig. 5 Magnified back reflection topographic image from Fig. 1(b) and a corresponding HRXRD map with the w rocking axis parallel to the radial boundaries.

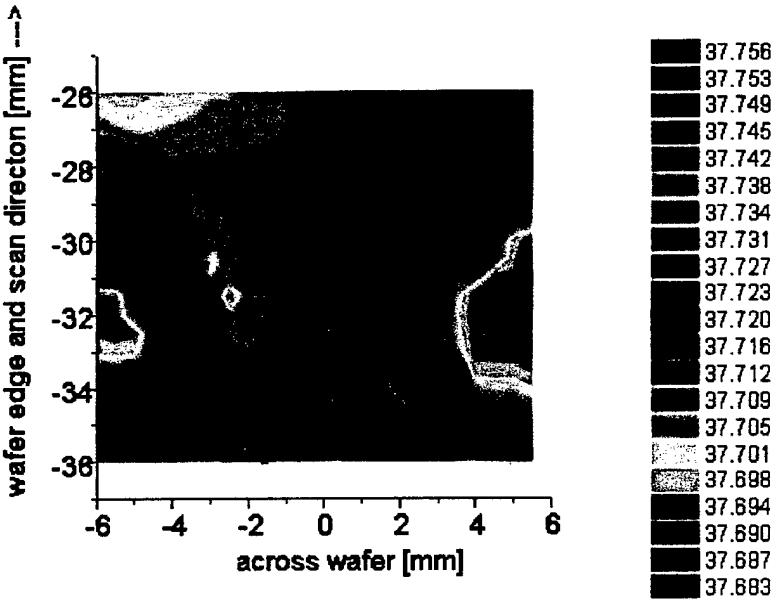

Fig. 6 HRXRD map of w peak position with rocking axis perpendicular to the boundary direction.

The remaining question is the origin of the defect arrays responsible for the observed misorientations. The most likely mechanism appears to be radial buckling od a rigidly mounted seed on the graphite crucible lid. This is possible considering that buckling has been observed in SiC at moderate temperatures [3]. It is also possible that the dark lines could represent the effect of polygonization of basal plane dislocations [4]. Further work is required to distinguish between these two plausible mechanisms.

References

[1]W.Si, M. Dudley, C. Carter, R. Glass, and V. Tsvetkov, Mat. Res. Soc. Symp. Proc. 437(1996), p.129.

[2]K. Wessel and H. Alexander, Phil. Mag. 35 (1977), p.1523.

[3]S. Fugita, K. Maeda, and S.Hyodo, Phil. Mag. A 55, No.2 (1987), p.203.

[4]S. Ha, N.T. Nuhfer, G.S. Rohrer, M. De Graef, and M. Skowronski, this proceedings.

Hexagonal platelet-shape voids

A common defect in sublimation grown SiC boules is the hexagonal void; a flat, hexagonal, platelet-shaped cavity in the crystal that often has a hollow tube trailing beneath it. Although several groups have reported the observation of hexagonal voids, their morphology and effect on the growing crystal has not been described in detail. The focus of this work is to present evidence of void formation mechanism, their axial and lateral motion during growth, and to study the redistribution of defects caused by void passage.

A. Void Morphology and Movement

Fig. 7 shows optical micrographs of a typical hexagonal void in planar view (a) and a similar void in cross-section (b). The wafer imaged in Fig. 7(a) was cut perpendicular to the growth direction from a boule grown on the Si-face of the seed, and shows that the void lays parallel to the SiC basal planes. The void is enclosed in the crystal and imaged in reflection by looking down the growth direction towards the seed. Fig. 7(b) is a reflection image of an axial cut slice that has been polished down to open a void. The void in Fig. 7(b) shows a typical 6 mm void thickness with trench-like depressions on both sides. In the remainder of this report, the top of the void will be defined as the void facet that is closest to the growth surface, and the bottom of the void is the facet that is closest to the seed (the bottom of the void and the boule growth surface face the same direction). Several features are apparent in Fig. 7(a): a relatively thick black border surrounding the void, large semicircular steps and terraces, and a black region near the left edge of the void. The black border around the void in Fig. 7(a) can be attributed to the slanted sidewalls at the top of the void that can be seen in Fig. 7(b). Laue diffraction patterns of the sample containing the void revealed that the void edges lay perpendicular to the $<1\bar{1}00>$ directions. Focusing of the optical microscope at different depths showed that the terraces step down towards the left side of the void and terminate in a trench similar to those that extend beneath the void in Fig. 7(b). AFM scans of the bottoms of similar voids showed average step heights ranging from 100-500 Å. The convex shape of the steps as they decrease in elevation from the right to the left side of the image are consistent with the shape of the macrosteps on the SiC growth surface and indicate that the steps are due to growth on the bottom of the void. Macrosteps were usually observed on the void bottom when the crystal was grown on the Si-face, while smaller unit cell-sized steps were usually observed on the void bottom in crystals grown on the C-face. This result is consistent with the results reported by Takahashi and Okamoto, who showed the preference for macrostep formation on the Si-face of PVT-grown SiC.

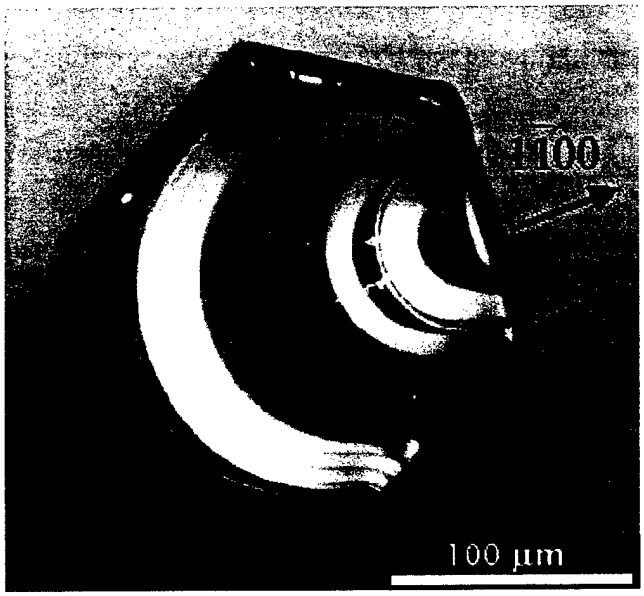

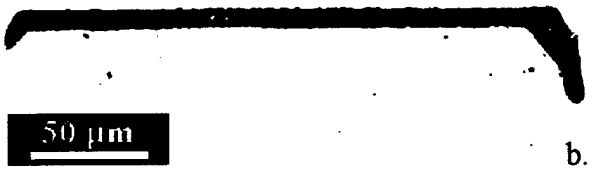

b.

Fig. 7 Optical microscopy images showing plan view (upper) and cross section (bottom) of the hexagonal void in PVT SiC wafer.

Fig. 8 contains planar view images of the top of a hexagonal void that was observed in a crystal grown on the C-face of a seed, thus are images of the Si-face. Fig. 8(a) is a reflection optical micrograph of a void that has been polished open from the bottom, showing almost concentric terraces and polishing damage on the left side of the image. Focusing of the optical microscope revealed that the terraces step up toward the outer edges of the void, leaving a central depression. Fig. 8(b) is an AFM scan of a region near the center of the depression in Fig. 8(a). White spots are polishing related deposits that could not be removed during cleaning, and the black feature at the bottom of the image is a scratch produced during opening of the void. Smaller 15 Å high steps spiral around screw dislocations terminating at the void top surface. Steps decrease in elevation in a

clockwise circuit around the dislocations, and have a concave step front, indicating that they are evaporation steps rather than growth steps. Similar to the growth steps, evaporation steps were macroscopic on the Si top surface of a void observed in a boule grown on the C seed face (as seen in Fig. 8a), while smaller unit cell-sized steps were observed on the C top surface of a void observed in a boule grown on the Si seed face. The presence of both growth steps on the bottom of the void and evaporation steps at the top of the void provide strong evidence for the motion of hexagonal voids during sublimation growth.

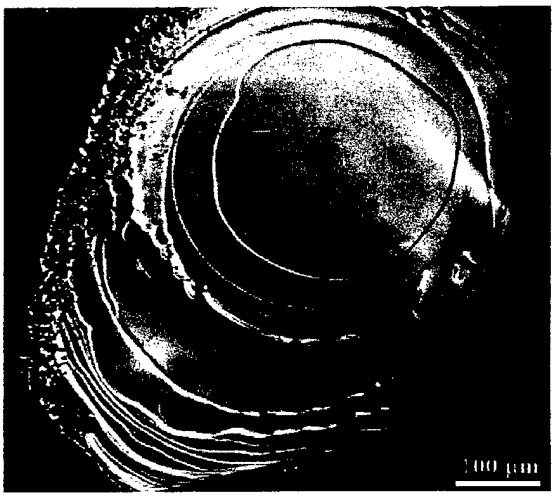

Fig. 8. (a) Optical micrograph of the top facet of a hexagonal void that was polished open. The crystal was grown on the C-face. Steps move outwards from the center of the facet, with the center being the lowest elevation in the image.

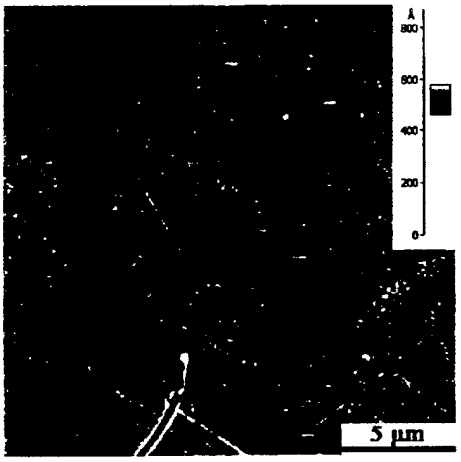

Fig. 8 (b) AFM image near the center of the depression shown in (a). Spiral etching steps spin around several screw dislocations. Step heights are ~ 15 Å.

Fig. 9 shows images of the early stages of hexagonal void formation in a short growth experiment. A Lely seed was attached to a graphite crucible cap using sucrose as an attachment layer. The crucible bottom and top temperatures were 2200 °C and 2090 °C, respectively. The argon growth pressure was 2 torr, yielding a growth rate of approximately 0.5 mm/hr. The growth was interrupted after 8 hours in order to see the formation of hexagonal voids. After growth, the crystal was removed from the cap by grinding away most of the graphite and oxidizing the remaining material. The interface between the seed and crucible cap is shown in Fig. 9. Fig. 9(a) is an optical image in reflection of a hexagonal depression with dimensions similar to that of a hexagonal void that can be found in crystals grown for a long time. The depression has an out of focus region in the center that corresponds to the top of the void, and black features that are areas of incomplete evaporation, as can be seen in Fig. 9(b). The void takes on a hexagonal shape immediately at the seed / lid interface with edges perpendicular to $<1\bar{1}00>$ directions. It is apparent that the void formed because of an imperfection or cavity in the attachment layer, and that transport occurred across the cavity in a manner similar to the transport during PVT growth. At the left and right edges of the void are regions (N) that protrude sideways into the void interior. Fig. 9(b) is a SEM micrograph showing a close-up of an (N) region seen on the left side of Fig. 9(a). The protrusion is an overhang that is not directly connected to the top of the void, and is most likely the initial stage of formation of the void bottom. The overhang has the same orientation as the surrounding crystal, as determined by orientation imaging microscopy. Sidewall nucleation and growth is supported by the lack of significant misorientation. If nucleation and growth had occurred on the crucible cap, then it would be expected that the volume beneath the void would be highly misoriented.

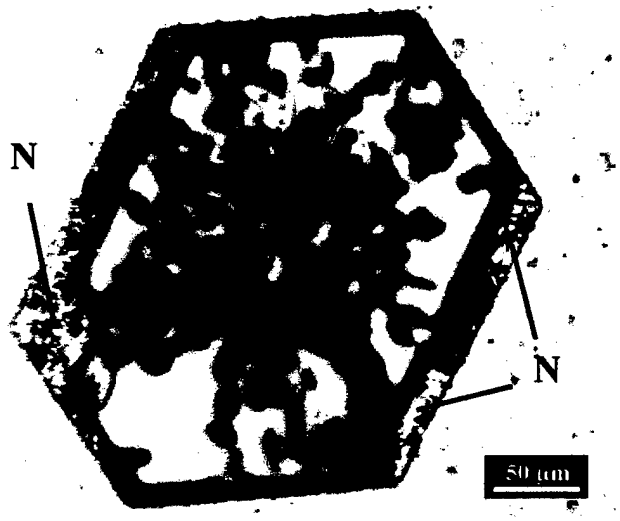

a

Fig. 9. Optical (a) and SEM (b) micrographs of void formation at the seed / crucible interface. Regions (N) are overhangs that protrude into the void interior.

Interaction between voids and dislocations

Fig. 10 is a pair of optical micrographs taken from the same location on 2 adjacent wafers that were cut from a boule grown on the Si-face. The Si face has been polished and KOH etched. Each image is taken looking down the growth axis towards the seed. Fig. 10(a) shows etch pits on the wafer containing a void that has yet to pass through the etched Si-face, where the elongated bright hexagonal area is the void imaged beneath the surface. Fig. 10(b) shows the etch pit pattern on a wafer where the void has already passed through the etched Si face and is one wafer closer to the seed. In both images, there are several features that confirm that the same area is being imaged. There are sets of parallel lines that can be attributed to polygonized dislocation arrays (A), and a pair of micropipes (M). Below the void (Fig. 10b), etch pits line up along the edges of the void path, and larger etch pits reside at the corners. Examination of the areas in Fig. 10 at a higher magnification allowed for determination of dislocation etch pit types according to the studies done by Takahashi et al. The smaller pits delineating the void trace are a mixture of threading edge and screw dislocations, and the larger dark pits are due to micropipes. Different voids were observed to have different linear densities of dislocations associated with the trace of the void path. Dislocations found along the trace of the void path are further evidence that void movement has occurred and that void movement can rearrange dislocations by recrystallization.

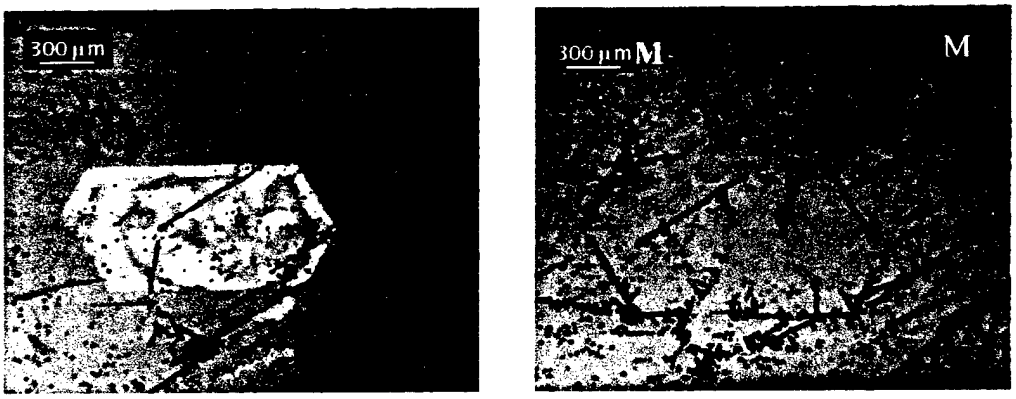

Fig. 10 Etch patterns of 2 adjacent wafers taken from a crystal grown on the Si-face: (a) contains the void, and the etch surface is above it; (b) is a wafer closer to the seed. Etch pits line up along the sidewalls of the void path, and larger hexagonal pits reside at the corners.

Screw dislocation distributions above and below the location of the void in the crystal were assessed using synchrotron white-beam x-ray topography. Back-reflection topographs of SiC on-axis wafers show images of threading screw dislocations that consist of black rings encompassing white circles, with the diameters of the rings proportional to the screw dislocations' Burgers vector. The Burgers vectors of these dislocations can occur in multiples of the crystal's c-lattice parameter; the smallest, having strengths of 1**c**, are termed elementary screw dislocations, and the larger are often called superscrew dislocations. Superscrew dislocations with a Burgers vector greater than 3**c** have hollow cores and are referred to as micropipes. Fig. 11(a) shows a back-reflection topograph of the area above a void, and Fig. 11(b) shows the same area below the void. The area the void will pass through is outlined in white in Fig. 11(a), and the hexagon of light and dark orientation contrast that occupies the center of Fig. 11(b) represents the trace of the void's path through the crystal during boule growth. Large white spots to the left and lower right of the hexagon in both images are micropipes present in both wafers. The average screw dislocation density in Fig. 11(a) is 5.5×10^3 cm^{-2}, and the area delineated by the hexagon directly above the void in Fig. 11(a) contains 15 elementary screw dislocations. Outside the void path in Fig. 11(b) the dislocation density is the same as in Fig. 11(a), but within that there are no screw dislocations. Reflection optical micrographs of etched surfaces above and below the void confirmed the absence of elementary screw dislocations and the presence of micropipes. Since the dislocation density outside the void path has not significantly changed, it can be assumed that the void has provided a mechanism for the rearrangement of single screw

dislocations and the formation of micropipes. In addition, both the surrounding wafer and the area within the void trace are imaged at the same time during x-ray topography. This indicates that the misorientations associated with recrystallization are small, and further supports the argument that growth behind the void did not initiate by independent nucleation on the crucible cap.

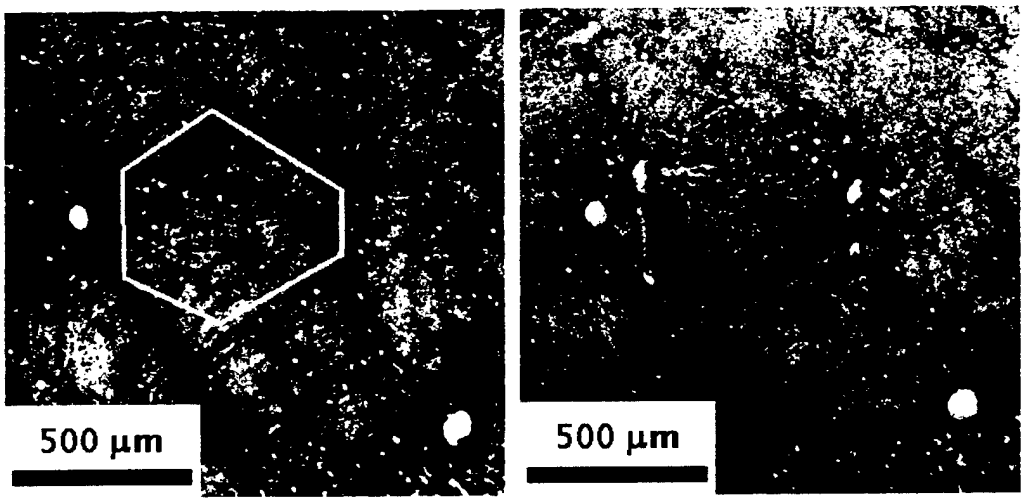

Fig. 11. Back-reflection x-ray topographs (**g** = 00024, λ = 1.24 Å) of the area above a void (a), and below a void (b). The projected passage of the void has been traced in white. The screw dislocations visible above the void in (a) are not visible beneath the void in (b).

Fig. 13 is a schematic representation of the void and micropipe formation process. The PVT-grown wafers used as seeds typically contain 10^4 cm^{-2} threading edge dislocations and 10^3-10^4 cm^{-2} elementary screw dislocations. The void moves into the crystal and immediately intersects dislocations, which now terminate at the top of the void still open to the back of the crystal. Nucleation occurs at the sidewall of the void, as can be seen in Fig. 8, and the void begins to close as it moves into the crystal. It is well known that dislocation lines cannot end inside a crystal; they must terminate at a b r dislocation or a free surface. Although the interior of a void may be considered a free surface, an enclosed cavity must have a net Burger's vector of zero. If the cavity surface divides in two (in our case the top and bottom void facets), then the net Burger's vector of each half must be equal. Consequently, if the net Burger's vector of dislocations terminating at the top of the void is not zero, then dislocations must be created in the recrystallized material beneath the void. This conserves the net Burgers vector between the top and bottom of

the void. Dislocations will likely form in the last closed regions of the void bottom where the convex growth front makes a hole with the angled corners of the void walls. Only basal plane dislocations should propagate into the growth homogenously nucleated at a void sidewall; stresses, foreign material, and high supersaturations that normally result in dislocation formation are not present. In addition, the growth front of the closing void bottom does not initially have any support from either above or below. The cantilevered growth front could flex up or down under the influence of small forces, which in turn would cause the formation of additional dislocations not already present in the seed. Similarly, this effect was observed in the pendeo-epitaxy of GaN, where cantilevered lateral growth fronts contact to produce rows of dislocations. The strain associated with a dislocation increases the bond energy near the dislocation core, which in turn can lower the probability of adatom attachment. The growth rate near a dislocation is therefore expected to be slower. This leads to the formation of a trench opposite to the nucleation site. As the trench gets deeper, the temperature at its bottom will be colder than the rest of the void. Local supersaturation will eventually cause the trench to close, as discussed by Benema. The formation of a trench is also seen in GaN pendeo-epitaxy where the mating growth fronts do not completely close beneath the elevated GaN seeds.

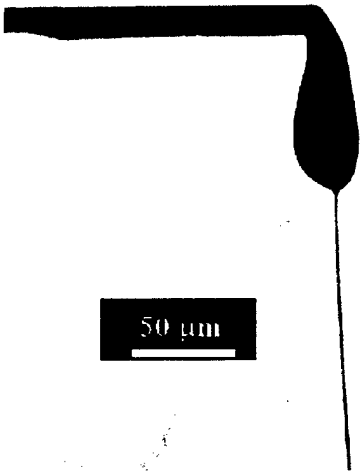

Fig. 12 Micropipe extended below the trench formed at the bottom of hexagonal void. This is the dominant formation mechanism for micropipes.

In order for screw dislocations to combine and micropipes to form, the dislocations must be forced together. The depressions that occur at the corner of the void, formed by the last closing regions of the growth front in the trench, provide the location for screw

dislocations to combine. If screw dislocations are in the region of the depression when it begins to close, then it is energetically more stable for the dislocation core to remain open because the surface energy of the open core is less than that of the strain energy of the closed core. The image forces associated with the large growth steps can push additional screw dislocations lined up in the trench along the edge of the void closer to the depressions at the void corners. According to Pirouz, once a dislocation is close enough (~5 nm) to a hole already containing a dislocation of the same sign (effectively a micropipe), then the force between the closed-core screw dislocation and open-core screw dislocation becomes attractive. Same-sign dislocations can combine in the hole, thus forming a micropipe at the bottom of a trench extending below the void.

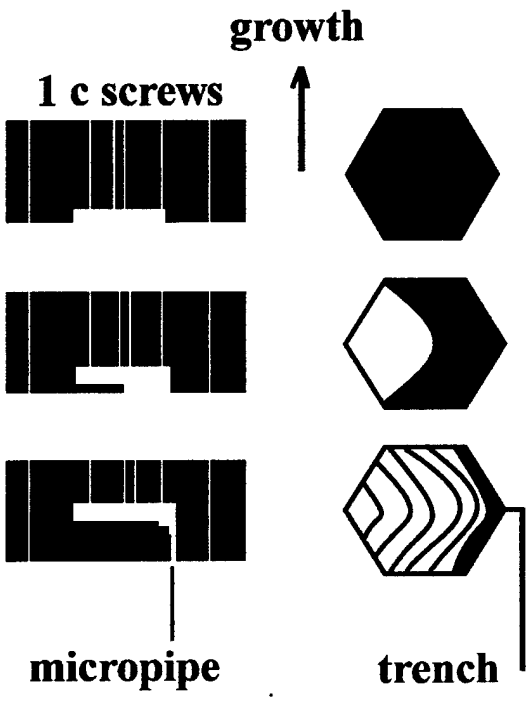

Fig. 13 Schematic diagram showing void formation and movement. The void begins as a cavity in the seed attachment layer, growth within the void occurs by lateral attachment and step flow, and the trench closes at the corners of the void, forming micropipes that extend beneath the void.

Hexagonal voids approximately 300 μm on a side moving in a crystal with an elementary screw dislocation density of $1x10^4$ cm^{-2} will intersect approximately 10 elementary screw dislocations. The results presented in this paper show that elementary screw dislocations result in micropipes that extend beneath the void. If we assume that there are 3

micropipes created per void, and then consider the density of hexagonal defects in the wafers obtained (1-5 cm^{-2}), it is possible to have micropipe densities in a single wafer of 3-15 cm^{-2} simply because of hexagonal voids. In addition, hexagonal voids are distributed throughout the boule, which leads to higher micropipe densities closer to the seed. If we assume a boule length of one inch (50 times greater than the wafer thickness), then it is possible that wafers near the seed have micropipe densities between 150 and 750 cm^{-2}. Since the micropipe density in wafers is ~100 cm^{-2}, voids could be the dominant formation mechanism for micropipes. The likelihood that they move laterally in addition to axially further supports that this mechanism for micropipe formation is likely to be dominant in any crystal that contains hexagonal voids. Elimination of hexagonal voids by use of a backside evaporation barrier and proper seed mounting techniques was shown to reduce micropipe densities in PVT grown SiC.

The formation mechanism of hexagonal voids and micropies identified above provided an insight of how to suppress their formation. The key to preventing them is to form a continuous diffusion barrier for silicon bearing species. An approach relying on deposition of a thin graphite layer was tested. The backside of one seed crystal was painted with photoresist, approximately 15 μm thick, cured in a furnace at a temperature of 120°C for 5 min, and annealed in high vacuum (< $3x10^{-7}$ torr) at a temperature of 1200°C, utilizing a temperature ramp rate of 400°C/h. The resulting carbon protection layer was shiny and contained no visible cracks or voids. A seed crystal with the protection layer applied to its backside and an unprotected seed crystal were mounted side by side on the same crucible lid using the standard carbonized sucrose attachment layer. Both crystals were overgrown simultaneously in the same PVT growth experiment at a temperature of 2300°C, with gradient of 10 K/cm, under an argon pressure of 20 torr for 14 hours. An axial slice parallel to the growth direction (c- axis) was cut from the boule revealing both seed crystals.

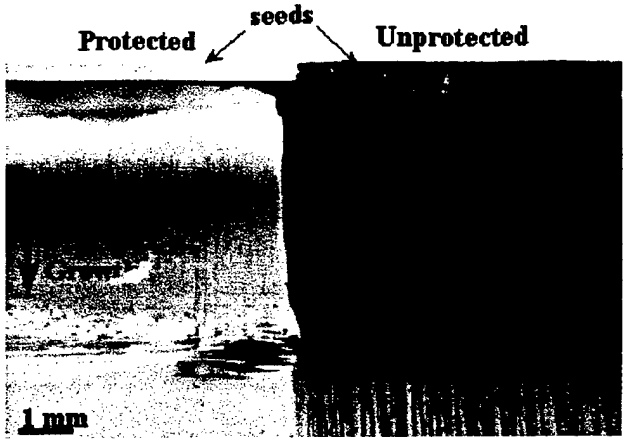

Fig. 14 Optical microscopy image of an axial slice through the SiC boule grown on two seeds. On left the seed backsurface was protected by a thin graphite layer. On right the SiC seed was attached to the crucible lid without protective layer.

Figure 14 shows an optical microscope image of the slice in transmitted light. The protected seed crystal is transparent and shows no signs of micropipes or macrodefects while the unprotected seed crystal has macrodefect cavities propagating though the entire crystal. It is apparent that the continuous graphite film on the backside of the protected seed suppressed the non-uniform sublimation. In the unprotected seed crystal (bottom image), thermal decomposition cavities originate at the seed/lid boundary between the seed and crucible lid. These features are not observed in the protected seed crystal. The protection layer eliminates the vapor diffusion path of Si. Silicon may still diffuse through the solid protective layer, however, this occurs at a rate which is much slower than the vapor transport and does not result in thermal decomposition cavities. It should also be mentioned that growth experiments conducted with a modified attachment technique that yielded continuous carbonized sucrose layers, containing no observable voids, resulted in crystals with no thermal decomposition cavities. However, formation of the homogeneous attachment layer using carbonized sucrose is not entirely reproducible. These preliminary results suggest that a sufficiently continuous attachment layer can act as a protection layer.

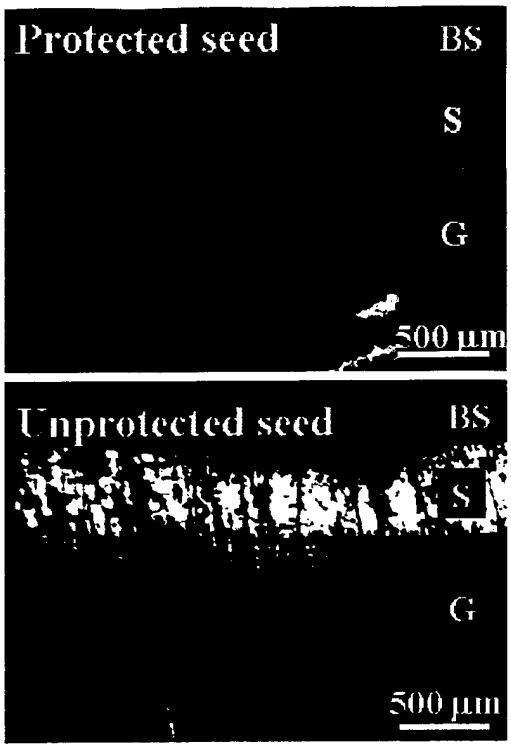

Fig. 15. Higher magnification optical cross-sectional images in transmitted light of the seed crystal/lid interfaces of the protected and the unprotected seed crystals shown in Fig. 14. BS marks the location of the seed backside, S is the Lely seed and G is the grown crystal.

PERSONNEL SUPPORTED:

Funding supported one graduate student, Edward Sanchez for one year and Thomas A. Kuhr, full time for two years.

PUBLICATIONS:

1. "Formation of thermal decomposition cavities in physical vapor transport of silicon carbide crystals" E. K. Sanchez , T. Kuhr, V. D. Heydemann, D. W. Snyder, G. S. Rohrer, and M. Skowronski, submitted to Journal of Electronic Materials.
2. "X-ray characterization of 3 inch diameter experimental 4H-SiC wafers", T. A. Kuhr, M. Skowronski, W. M. Vetter, and M. Dudley, accepted to Int. Conf. Silicon Carbide and Related Materials, Durham, NC, 1999.

3. "Nucleation of screw dislocations during physical vapor transport growth of silicon carbide", E. K. Sanchez, T. A. Kuhr, G. S. Rohrer, M. Skowronski, V. D. Heydemann, and D. W. Snyder, accepted to Int. Conf. Silicon Carbide and Related Materials, Durham, NC, 1999.

Interactions/Transitions

(a) Participation/presentations at meetings, conferences, seminars...

Results on thermal decomposition voids formation in SiC have been presented at the 1999 Electronic Materials Conference in Santa Barbara, CA, in June 99. Two papers have been presented at the premiere conference in the field of silicon carbide, namely International Conference on Silicon Carbide and Related Materials in Durham, NC in October 99. The results on hexagonal voids were presented at the American Association for Crystal Growth Conference in Vail, CO in August 2000. The results also have been presented at the seminar at Aitron Litton in Morristown NJ and UCAR Research Center in Parma OH in April and May of 2000.

(b) Consultative and advisory functions.

Preliminary results of structural characterization of SiC wafers have been presented to Tri-Service committee at the bidders conference for the Air Force Title III program (Wright-Patterson Air Force Base, October 98). Copies of abstracts and pre-prints of publications have been provided to AFRL researchers and program monitors: L. S. Rea, E. Stutz, J. Blevins, and W. C. Mitchel. The results were provided to Advanced Technology Materials, II-VI Inc., Airtron Litton, and Sterling Semiconductor.

(c) Transitions

The diffusion barrier layer technique has been transferred to II-VI, Inc. (Saxonburg, PA) and to Sterling Semiconductor, Inc. (Sterling, VA) where it is being tested and optimized for inclusion in the standard SiC growth process.

Discoveries, inventions, patent disclosures

None